Heterodinuclear $Cu^{II}Pb^{II}$ and $Cu^{II}M^{II}$ (M = Mn, Fe, Co, Ni, Cu, Zn) Complexes of Macrocycles with Dissimilar 4- and 5-Coordination Sites: Synthesis, Structures, and Properties

Hisashi Ōkawa,*[1a] Jun Nishio,[1a] Masaaki Ohba,[1a] Makoto Tadokoro,[1a,b] Naohide Matsumoto,[1a] Masayuki Koikawa,[1a,c] Sigeo Kida,[1a,d] and David E. Fenton[1e]

Departments of Chemistry, Faculty of Science, Kyushu University, Hakozaki, Higashiku, Fukuoka 812, Japan, and The University of Sheffield, Sheffield S3 7HF, England

Received November 18, 1992

Heterodinucleating macrocycles with two 2,6-bis(iminomethyl)-4-methylphenolate entities combined through two lateral chains, $-(CH_2)_2-$ and $-(CH_2)_mNH(CH_2)_m-$ ($m = 2, 3$), at the imino nitrogens have been prepared as $Cu^{II}Pb^{II}$ complexes of the formula [CuPb(L)]XY (L^{2-} = L1 for $m = 2$ and L2 for $m = 3$; XY = $(ClO_4)_2$, $(NO_3)(PF_6)$, $(AcO)(BPh_4)$). [CuPb(L1)](AcO)(BPh_4)·DMF crystallizes in the monoclinic crystal system, space group $P2_1/n$, with $Z = 4$, $a = 18.890(3)$ Å, $b = 19.968(3)$ Å, $c = 12.704(2)$ Å, $\beta = 91.61(1)°$, and $V = 4790(1)$ Å^3. The refinement converges with $R = 0.0697$ and $R_w = 0.0863$ for 4945 reflections with $|F_o| > 3\sigma(|F_o|)$. The crystal consists of a dimeric cation $\{CuPb(L1)(Ac)\}_2^{2+}$ bridged by acetate groups, tetraphenylborate ions, and DMF molecules. The Cu is located at the 4-coordination site formed with the ethylene chain and assumes a planar environment. The Pb is at the 5-coordination site formed with the $-(CH_2)_2NH(CH_2)_2-$ chain and assumes an eight-coordinate structure also involving three acetate oxygen atoms. The Cu- -Pb separation, bridged by two phenolic oxygens, is 3.577(2) Å. In the crystal, the dimeric cations further interact through out-of-plane bonding between the $\{CuN_2O_2\}$ entities forming a column along the a axis. The [CuPb(L1)]XY complexes react with metal(II) sulfates to form a series of $Cu^{II}M^{II}$ complexes, [CuM(L1)]XY (M = Mn, Fe, Co, Ni, Cu, Zn). [CuMn(L1)](AcO)(BPh_4) crystallizes in the monoclinic space group $P2_1/n$, with $Z = 4$, $a = 17.508(8)$ Å, $b = 15.539(5)$ Å, $c = 16.515(5)$ Å, $\beta = 106.30(3)°$, and $V = 4312(3)$ Å^3. The refinement converges with $R = 0.0689$ and $R_w = 0.0563$ for 2935 reflections with $|F_o| > 3\sigma(|F_o|)$. The Cu(II) and Mn(II) ions reside at the 4- and 5-coordination sites of the macrocycle, respectively, and the acetate group bridges the two metal ions providing a nearly square-pyramidal geometry for the Cu and a highly distorted six-coordinate environment for the Mn. The Cu- -Mn separation is 3.122(2) Å. The cryomagnetic investigations (4.2–300 K) for the CuMn, CuFe, CuCo, CuNi, and CuCu complexes reveal the operation of an antiferromagnetic spin-exchange interaction within each molecule. The cyclic voltammograms of the CuM complexes show Cu(II)/Cu(I) reduction near –0.8 V (vs SCE) and oxidation at the ligand center near +1.3 V. The oxidation of the Fe(II) of the CuFe complex occurs at +0.64 V whereas the Mn(II) ion of the CuMn complex and the Co(II) ion of the CuCo complex are hardly oxidized.

Introduction

The design of dinucleating ligands that incorporate dissimilar metal ions to form discrete heterodinuclear complexes is of importance in attempts to mimic the active sites of metalloenzymes such as cytochrome *c* oxidase[2] and bovine erythrocyte superoxide dismutase[3] and to search appropriate systems for binding and activating simple molecules[4-6] and in investigations concerning the mutual influences of two metal centers on the electronic, magnetic, and electrochemical properties of such heterodinuclear systems.[7,8] Dinucleating macrocyclic ligands with dissimilar coordination sites are of particular importance because heterodinuclear complexes derived from such macrocycles are thermodynamically stabilized and kinetically retarded with regard to metal dissociation and metal substitution relative to metal complexes of acyclic ligands (the macrocyclic effect).[9] Further, macrocyclic ligands can provide a well-defined environment for the bound metal ions and influence their physicochemical properties.[10]

The dinucleating macrocycles derived from the 2:2 condensation of 2,6-diformyl-4-methylphenol and 1,3-diaminopropane (see Chart I, structure I, $m = n = 3$) was first obtained by Pilkington and Robson[11] in a one-pot reaction of the components in the presence of an appropriate metal ion (direct template reaction). Shortly thereafter we[12] reported the synthesis of macrocycles with different lateral chains (structure I; $m \neq n$) by the stepwise cyclization using two dissimilar alkanediamines (stepwise template reaction). Macrocycles of type I have been extensively used for studies of homo- and heterodinuclear complexes and mixed-

(1) (a) Kyushu University. (b) Present location: The Institute for Molecular Science, Myodaiji, Okazaki 444, Japan. (c) Present location: Department of Chemistry, Faculty of Science and Engineering, Saga University, Saga 840, Japan. (d) Present location: Kumamoto Institute of Technology, Ikeda 4-22-1, Kumamoto 860, Japan. (e) The University of Sheffield.

(2) Palmer, G.; Babcock, G. T.; Vickery, L. E. *Proc. Natl. Acad. Sci. U.S.A.* **1976**, *73*, 2206. Babcock, G. T.; Vickery, L. E.; Palmer, G. *J. Biol. Chem.* **1978**, *253*, 2400.

(3) Richardson, J. S.; Thomas, K. A.; Rubin, B. H.; Richardson, D. C. *Proc. Nat. Acad. Sci. U.S.A.* **1975**, *72*, 1349.

(4) Vigato, P. A.; Tamburini, S.; Fenton, D. E. *Coord. Chem. Rev.* **1990**, *106*, 25.

(5) Gambarotta, S.; Arena, F.; Floriani, C.; Zanazzi, P. F. *J. Am. Chem. Soc.* **1982**, *104*, 5082. Arena, F.; Floriani, C.; Chiesi-Villa, A.; Guastini, C. *Inorg. Chem.* **1986**, *25*, 4589.

(6) Sakamoto, M.; Takagi, M.; Ishimori, T.; Ōkawa, H. *Bull. Chem. Soc. Jpn.* **1988**, *61*, 1613. Sakamoto, M.; Ishimori, T.; Ōkawa, H. *Ibid.* **1988**, *61*, 3319. Aratake, Y.; Ōkawa, H.; Asato, E.; Sakiyama, H.; Kodera, M.; Kida, S.; Sakamoto, M. *J. Chem. Soc., Dalton Trans.* **1990**, 2941.

(7) Kahn, O. *Struct. Bonding (Berlin)* **1987**, *68*, 89. Sinn, E.; Harris, C. M. *Coord. Chem. Rev.* **1969**, *4*, 391.

(8) Casellato, U.; Vigato, P. A.; Vidali, M. *Coord. Chem. Rev.* **1977**, *23*, 31. Zanello, P.; Tamburini, S.; Vigato, P. A.; Mazzocchin, G. A. *Ibid.* **1987**, *77*, 165.

(9) Cabbines, D. K.; Margerum, D. W. *J. Am. Chem. Soc.* **1969**, *91*, 6450. Lamb, J. D.; Izatt, R. W.; Christensen, J. J.; Eatough, D. J. In *Coordination Chemistry of Macrocyclic Compounds*; Melson, G. A., Eds.; Plenum Press: New York, 1979; p 145.

(10) Endicott, J. F.; Durham, B. In *Coordination Chemistry of Macrocyclic Compounds*; Melson, G. A., Eds.; Plenum Press: New York, 1979; p 393.

(11) Pilkington, N. H.; Robson, R. *Aust. J. Chem.* **1970**, *23*, 2225.

(12) Ōkawa, H.; Kida, S. *Inorg. Nucl. Chem. Lett.* **1971**, *7*, 751. Ōkawa, H.; Kida, S. *Bull. Chem. Soc. Jpn.* **1972**, *45*, 1759.

0020-1669/93/1332-2949$04.00/0

Chart I

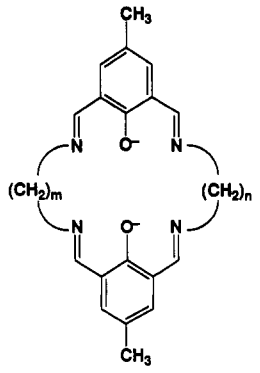

I

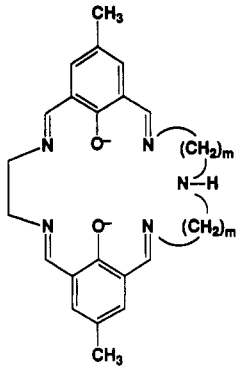

II

valence complexes.[13-17] Related heterodinucleating macrocycles have been prepared by Casellato et al.[18] by a similar stepwise template reaction, and more elaborate macrocyclic analogs with six-coordination sites have recently been obtained for studies of heterodinuclear complexes.[19,20]

Recently we[21,22] have found that the modified stepwise template reaction that requires two kinds of metal ions (Cu^{2+} (or Ni^{2+}) and Pb^{2+}) at the two different steps in the cyclization reaction can be applied to the synthesis of the nonsymmetric macrocycles I with a wide range of (m, n) sets and their analogs with an alcoholic group as a potent donor group on one lateral chain. In this study, new heterodinucleating macrocycles with two 2,6-bis(iminomethyl)-4-methylphenolate entities combined through two lateral chains, $-(CH_2)_2-$ and $-(CH_2)_mNH(CH_2)_m-$ (m = 2, 3), at the imino nitrogens (see structure II) have been prepared as dinuclear $Cu^{II}Pb^{II}$ complexes [CuPb(L)]XY (L^{2-} = L1 for m = 2 and L2 for m = 3; XY = $(ClO_4)_2$, $(NO_3)(PF_6)$, $(AcO)(BPh_4)$) by the modified stepwise template reaction. The macrocycles L1 and L2 bear a 4-coordination site with the N_2O_2 donor set and a 5-coordination site with the N_3O_2 donor set, sharing the bridging phenolic oxygen atoms. The structure of [CuPb(L1)](AcO)(BPh_4)·DMF has been determined by single-crystal X-ray crystallography. Further, a series of $Cu^{II}M^{II}$ complexes [CuM(L1)]XY (M = Mn, Fe, Co, Ni, Cu, Zn) have been prepared using [CuPb(L1)]XY as the precursor complexes. The characterization and properties of the heterodinuclear CuM complexes are reported together with the crystal structure of [CuMn(L1)](AcO)(BPh_4).

Experimental Section

Physical Measurements. Elemental analyses (C, H, and N) were obtained from the Service Center of Elemental Analysis at Kyushu University. Analyses of Mn, Fe, Co, Ni, Cu, and Zn were made on a Shimadzu AA-680 atomic absorption/flame emission spectrophotometer. Infrared spectra were recorded on a JASCO IR-810 spectrophotometer using KBr disks or Nujol mulls. Electronic spectra were measured on a Shimadzu UV-210 spectrophotometer at room temperature. Magnetic susceptibilities were measured on a Faraday balance in the temperature range 80–300 K and on a HOXAN HSM-D SQUID susceptometer in the range 4.2–80 K. Cyclic voltammograms were recorded on an apparatus comprising a Hokuto Denko HA-501 potentiostat and a HB-104 function generator. Measurements were carried out in acetonitrile or dimethyl sulfoxide (DMSO) solutions (ca. 1×10^{-3} M) containing tetraethylammonium perchlorate (TEAP, ca. 1×10^{-1} M) as the supporting electrolyte. (*Caution: TEAP is explosive and should be handled with great care!*) A three-electrode cell equipped with a glassy-carbon working electrode, a platinum coil as the auxiliary electrode, and a saturated calomel electrode as the reference was used. Controlled-potential electrolyses were made on the same apparatus using a platinum net as the working electrode. X-Band ESR spectra were recorded on a JES-FE3X spectrometer.

Syntheses. 2,6-Diformyl-4-methylphenol was prepared by the modified Duff reaction.[12,23] *N,N'*-Ethylenebis(3-formyl-5-methylsalicylideneamine), *N,N'*-1,3-propylenebis(3-formyl-5-methylsalicylideneamine), and their mononuclear copper(II) complexes were obtained by the literature methods.[12] *Caution: the perchlorate complexes described below may be explosive and should be handled with great care!*

[CuPb(L1)](ClO$_4$)$_2$·H$_2$O (1a). A mixture of [*N,N'*-ethylenebis(3-formyl-5-methylsalicylideneaminato)]copper(II) (1.0 g, 2.4 mmol), $Pb(ClO_4)_2·3H_2O$ (1.1 g, 2.4 mmol), and diethylenetriamine (0.25 g, 2.4 mmol) in methanol (70 cm^3) was refluxed to form a reddish clear solution from which reddish brown microcrystals were precipitated. They were separated by filtration, washed successively with methanol and ether, and dried in air. Yield: 0.88 g (97%). Anal. Calcd for $C_{24}H_{29}Cl_2CuN_5O_{11}Pb$: C, 31.86; H, 3.23; N, 7.74; Cu, 7.02. Found: C, 31.81; H, 3.23; N, 7.69; Cu, 6.88. μ_{eff}: 1.90 μ_B at 290 K. UV–vis data [λ/nm (ϵ/M^{-1} cm^{-1})] in acetonitrile: 376 (14 800), 549 (190). Selected IR data [ν/cm^{-1}] using KBr disks: 3320, 1638, 1625, 1138, 1105, 1082, 1050.

[CuPb(L1)](NO$_3$)(PF$_6$) (1b). This complex was obtained in a way similar to that of **1a** using $Pb(NO_3)_2·3H_2O$ instead of $Pb(ClO_4)_2·3H_2O$. Recrystallization from an acetonitrile–DMF (2:1 in volume) mixture formed reddish brown microcrystals. Yield: 73%. Anal. Calcd for $C_{24}H_{27}CuF_6N_6O_5PPb$: C, 32.20; H, 3.04; N, 9.39; Cu, 7.01. Found: C, 32.56; H, 3.28; N, 9.57; Cu, 6.85. μ_{eff}: 1.98 μ_B at 290 K. UV–vis data [λ/nm (ϵ/M^{-1} cm^{-1})] in DMF: 378 (13 200), 578 (210). Selected IR data [ν/cm^{-1}] using KBr disks: 3345, 1642, 1625, 1382, 840.

[CuPb(L1)](AcO)(BPh$_4$)·DMF (1c). A suspension of [*N,N'*-ethylenebis(3-formyl-5-methylsalicylideneaminato)]copper(II) (1.0 g, 2.4 mmol) in DMF (20 cm^3) and a solution of $Pb(AcO)_2·3H_2O$ (0.91 g, 2.4 mmol) in DMF (50 cm^3) were mixed and stirred at ambient temperature for 15 min. A DMF solution (20 cm^3) of diethylenetriamine (0.25 g, 2.4 mmol) was added, and the mixture was stirred for 30 min. $NaBPh_4$ (0.83 g, 2.4 mmol) was then added, and the mixture was refluxed with stirring. The resulted clear solution was concentrated to ca. 10 cm^3, diluted with acetonitrile (10 cm^3), and diffused with diethyl ether to give dark red crystals. They were recrystallized from an acetonitrile–DMF (2:1 in volume) mixture to form large crystals suitable for X-ray structure analysis. Yield: 0.88 g (79%). Anal. Calcd for $C_{52}H_{53}BCuN_6O_4Pb$: C, 56.39; H, 4.82; N, 7.59; Cu, 5.74. Found: C, 56.73; H, 4.84; N, 7.74; Cu, 5.74. μ_{eff}: 1.96 μ_B at 290 K. UV–vis data [λ/nm (ϵ/M^{-1} cm^{-1})] in acetonitrile: 378 (13 000), 572 (220). Selected IR data [ν/cm^{-1}] using KBr disks: 3250, 1640, 1620, 1542, 1438, 702.

[CuPb(L2)](ClO$_4$)$_2$·H$_2$O (2). [*N,N'*-ethylenebis(3-formyl-5-methylsalicylideneaminato)]copper(II) (1.0 g, 2.4 mmol), dipropylenetriamine (0.32 g, 2.4 mmol), and $Pb(ClO_4)_2·3H_2O$ (1.11 g, 2.4 mmol) were mixed in acetonitrile (70 cm^3) and stirred at ambient temperature for 1 h. The resulting reddish solution was concentrated to 20 cm^3 and diffused with ether to give dark red crystals. They were separated by filtration, washed with ether, and dried in air. Yield: 0.51 g (55%). Anal. Calcd for $C_{26}H_{33}Cl_2CuN_5O_{11}Pb$: C, 33.46; H, 3.56; N, 7.50; Cu, 6.81. Found: C, 33.32; H, 3.53; N, 7.51; Cu, 6.22. μ_{eff}: 1.90 μ_B at 290 K. UV–vis data [λ/nm (ϵ/M^{-1} cm^{-1})] in acetonitrile: 381 (9400), 549 (190). Selected IR data [ν/cm^{-1}] using KBr disks: 3275, 1650, 1620, 1105, 1090, 1075, 1050.

[CuMn(L1)](ClO$_4$)$_2$·H$_2$O·CH$_3$OH (3a). An acetonitrile solution (20 cm^3) of **1a** (0.91 g, 1.0 mmol) and a methanol solution of $MnSO_4·6H_2O$ (0.26 g, 1.0 mmol) were mixed, stirred at ambient temperature for 1 h, and evaporated to dryness. The residue was extracted with methanol (30

(13) Addison, A. W. *Inorg. Nucl. Chem. Lett.* **1976**, *12*, 899.
(14) (a) Gagne, R. R.; Koval, C. A.; Smith, T. J. *J. Am. Chem. Soc.* **1977**, *99*, 8367. (b) Gagne, R. R.; Koval, C. A.; Smith, T. J.; Cimolino, M. C. *Ibid.* **1979**, *101*, 4571. (c) Gagne, R. R.; Spiro, C. L.; Smith, T. J.; Hamann, C. A.; Thies, W. R.; Shiemke, A. K. *Ibid.* **1981**, *103*, 4073. (d) Spiro, C. L.; Lambert, S. L.; Smith, T. J.; Duesler, E. N.; Gagne, R. R.; Hendrickson, D. N. *Inorg. Chem.* **1981**, *20*, 1229. (e) Lambert, S. L.; Spiro, C. L.; Gagne, R. R.; Hendrickson, D. N. *Ibid.* **1982**, *21*, 68.
(15) Long, R. C.; Hendrickson, D. N. *J. Am. Chem. Soc.* **1983**, *105*, 1513.
(16) Mandal, S. K.; Nag, K. *J. Chem. Soc., Dalton Trans.* **1983**, 2429. Mandal, S. K.; Nag, K. *Ibid.* **1984**, 2141. Mandal, S. K.; Adhikary, B.; Nag, K. *Ibid.* **1986**, 1175.
(17) Hoskins, B. F.; Robson, R.; Williams, G. A. *Inorg. Chim. Acta* **1976**, *16*, 121. Hoskins, B. F.; Williams, G. A. *Aust. J. Chem.* **1975**, *28*, 2593, 2607.
(18) Caselato, U.; Fregona, D.; Sitran, S.; Tamburini, S.; Vigato, P. A. *Inorg. Chim. Acta* **1985**, *110*, 181. Casellato, U.; Guerriero, P.; Tamburini, S.; Vigato, P. A. *Ibid.* **1986**, *119*, 215.
(19) Fraser, C.; Johnston, L.; Rheingold, A. L.; Haggerty, B. S.; Williams, G. K.; Whelan, J.; Bosnich, B. *Inorg. Chem.* **1992**, *31*, 1835.
(20) Timken, M. D.; Marritt, W. A.; Hendrickson, D. N.; Gagne, R. A. *Inorg. Chem.* **1985**, *24*, 4202.
(21) Tadokoro, M.; Ōkawa, H.; Matsumoto, N.; Koikawa, M.; Kida, S. *J. Chem. Soc., Dalton Trans.* **1991**, 1657.
(22) Tadokoro, M.; Sakiyama, H.; Matsumoto, N.; Kodera, M.; Ōkawa, H.; Kida, S. *J. Chem. Soc., Dalton Trans.* **1992**, 313.
(23) Denton, D. A.; Suschitzky, H. *J. Chem. Soc.* **1963**, 4741.

cm^3), and the methanol extract was once filtered to separate any insoluble materials and diffused with ether to give violet crystals: 0.60 g (76%). Anal. Calcd for $C_{25}H_{33}Cl_2CuMnN_5O_{12}$: C, 38.25; H, 4.23; N, 8.92; Cu, 8.10; Mn, 7.00. Found: C, 38.14; H, 4.21; N, 8.76; Cu, 7.97; Mn, 7.02. μ_{eff} per CuMn: 5.60 μ_B at 290 K. UV–vis data [λ/nm (ϵ/M^{-1} cm^{-1})] in acetonitrile: 364 (15 500), 547 (200). Selected IR data [ν/cm^{-1}] using KBr disks: 3340, 1650, 1640, 1110, 1085, 1050.

[CuMn(L1)](NO$_3$)(PF$_6$)·2CH$_3$CN (3b). An acetonitrile solution (20 cm^3) of **1b** (0.90 g, 1.0 mmol) and a methanol solution of $MnSO_4·6H_2O$ (0.26 g, 1.0 mmol) were mixed, and the mixture was stirred at room temperature for 1 h and then evaporated to dryness. The residue was extracted with acetonitrile (20 cm^3), and the extract was diffused with ether to give purple crystals. They were separated, washed successively with an ether–methanol (1:1 in volume) mixture and ether, and dried in air. Yield: 0.46 g (56%). Anal. Calcd for $C_{28}H_{33}F_6CuMnN_8O_5P$: C, 40.76; H, 4.03; N, 13.58; Cu, 7.70; Mn, 6.66. Found: C, 41.10; H, 4.17; N, 13.23; Cu, 7.81; Mn, 6.83. μ_{eff} per CuMn: 5.63 μ_B at 290 K. UV–vis data [λ/nm (ϵ/M^{-1} cm^{-1})] in acetonitrile: 365 (13 200), 542 (180). Selected IR data [ν/cm^{-1}] using KBr disks: 3350, 1645, 1440, 1330, 840.

[CuMn(L1)](AcO)(BPh$_4$) (3c). A solution of **1c** (1.11 g, 1.0 mmol) and $MnSO_4·6H_2O$ (0.26 g, 1.0 mmol) in methanol (40 cm^3) was stirred at room temperature for 3 h and evaporated to dryness. The residue was extracted with DMF (10 cm^3), and the extract was diffused with methanol (20 cm^3) to give blue-green crystals. They were dissolved in DMF, and the solution was layered with 2-propanol to form well-grown crystals: 0.62 g (68%). Anal. Calcd for $C_{50}H_{51}BCuMnN_5O_4$: C, 65.61; H, 5.62; N, 7.65; Cu, 6.94; Mn, 6.00. Found: C, 65.42; H, 5.58; N, 7.63; Cu, 7.10; Mn, 6.14. μ_{eff} per CuMn: 5.85 μ_B at 290 K. UV–vis data [λ/nm (ϵ/M^{-1} cm^{-1})] in acetonitrile: 372 (16 400), 577 (220). Selected IR data [ν/cm^{-1}] using KBr disks: 3330, 1645, 1640, 1575, 1440, 735, 700.

[CuFe(L1)](ClO$_4$)$_2$·H$_2$O (4). The suspension of **1c** (0.91 g, 1 mmol) and $FeSO_4·7H_2O$ (0.28 g, 1 mmol) in a deaerated mixture of acetonitrile (50 cm^3) and methanol (30 cm^3) was stirred at room temperature for 1 h. The resulting lead(II) sulfate was separated by filtration, and the filtrate was evaporated to dryness. The residue was crystallized from acetonitrile as brown microcrystals: 0.44 g (58%). Anal. Calcd for $C_{24}H_{29}Cl_2CuFeN_5O_{11}$: C, 38.24; H, 3.88; N, 9.29; Cu, 8.39; Fe, 7.30. Found: C, 38.37; H, 3.85; N, 9.28; Cu, 8.43; Fe, 7.41. μ_{eff} per CuFe: 4.86 μ_B at 290 K. UV–vis data [λ/nm (ϵ/M^{-1} cm^{-1})] in acetonitrile: 364 (12 300), 468 (490), 548 (210). Selected IR data [ν/cm^{-1}] using KBr disks: 3310, 1640, 1625, 1100, 1080, 1055.

[CuCo(L1)](ClO$_4$)$_2$·2H$_2$O (5a). The solution of **1a** (0.89 g, 1.0 mmol) and $CoSO_4·6H_2O$ (0.28 g, 1.0 mmol) in acetonitrile (20 cm^3) was stirred at room temperature for 1 h and evaporated to dryness. The residue was dissolved in methanol (20 cm^3), and the solution was diffused with ether to give purple prisms: 0.60 g (77%). Anal. Calcd for $C_{24}H_{31}Cl_2CoCuN_5O_{12}$: C, 37.20; H, 4.03; N, 9.03; Cu, 8.20; Co, 7.61. Found: C, 37.08; H, 3.61; N, 9.03; Cu, 7.91; Co, 7.58. μ_{eff} per CuCo: 4.57 μ_B at 290 K. UV–vis data [λ/nm (ϵ/M^{-1} cm^{-1})] in acetonitrile: 369 (11 900), 540 (170), 1115 (8). Selected IR data [ν/cm^{-1}] using KBr disks: 3310, 1650, 1635, 1105, 1080, 1050.

[CuCo(L1)](NO$_3$)(PF$_6$)·2H$_2$O (5b). The solution of **1b** (0.90 g, 1.0 mmol) and $CoSO_4·6H_2O$ (0.28 g, 1.0 mmol) in a mixture of acetonitrile (20 cm^3) and methanol (20 cm^3) was stirred at room temperature for 1 h and evaporated to dryness. The residue was dissolved in methanol (20 cm^3), and the solution was diffused with ether to give wine-red crystals: 0.64 g (82%). Anal. Calcd for $C_{24}H_{31}CoCuF_6N_6O_7P$: C, 36.82; H, 3.99; N, 10.73; Cu, 8.12; Co, 7.53. Found: C, 36.14; H, 3.89; N, 10.60; Cu, 8.15; Co, 7.82. μ_{eff} per CuCo: 4.50 μ_B at 290 K. UV–vis data [λ/nm (ϵ/M^{-1} cm^{-1})] in acetonitrile: 370 (12 300), 541 (180), 1110 (7). Selected IR data [ν/cm^{-1}] using KBr disks: 3340, 1645, 1620, 1320, 840.

[CuNi(L1)](ClO$_4$)$_2$·4H$_2$O (6). A solution of **1a** (0.91 g, 1.0 mmol) and $NiSO_4·6H_2O$ (0.26 g, 1.0 mmol) in a mixture of acetonitrile (40 cm^3) and methanol (20 cm^3) was stirred at ambient temperature for 1 h and filtered. The filtrate was diffused with dimethoxymethane in a desiccator to form deep red crystals: 0.51 g (63%). Anal. Found for $C_{24}H_{35}Cl_2CuN_5NiO_{14}$: C, 35.56; H, 4.35; N, 8.64; Cu, 7.84; Ni, 7.24. Found: C, 35.69; H, 4.06; N, 8.93; Cu, 7.75; Ni, 7.19. μ_{eff} per CuNi: 2.71 μ_B at 290 K. UV–vis data [λ/nm (ϵ/M^{-1} cm^{-1})] in acetonitrile: 367 (13 500), 527 (130), 1115 (11). Selected IR data [ν/cm^{-1}] using KBr disks: 3300, 1640, 1630, 1110, 1085, 1050.

[Cu$_2$(L1)](ClO$_4$)$_2$·0.5H$_2$O (7). This complex was obtained by the reaction of **1a** (0.91 g, 1.0 mmol) and $CuSO_4·5H_2O$ (0.25 g, 1.0 mmol) in a mixed solvent of acetonitrile (40 cm^3) and methanol (20 cm^3). The crude product was dissolved in acetonitrile (30 cm^3), and the solution was diffused with dimethoxymethane to form dark green crystals: 0.50 g (66%). Anal. Calcd for $C_{24}H_{28}Cl_2Cu_2N_5O_{10.5}$: C, 38.31; H, 3.75; N, 9.31; Cu, 16.89. Found: C, 38.20; H, 4.03; N, 9.55; Cu, 16.23. μ_{eff} per Cu: 1.64 μ_B at 290 K. UV–vis data [λ/nm (ϵ/M^{-1} cm^{-1})] in acetonitrile: 368 (10 100), 569 (290). Selected IR data [ν/cm^{-1}] using KBr disks: 3250, 1640, 1630, 1100.

[CuZn(L1)](ClO$_4$)$_2$·2H$_2$O·CH$_3$OH (8). A suspension of **1a** (0.91 g, 1.0 mmol) in acetonitrile (40 cm^3) and a solution of $ZnSO_4·7H_2O$ (0.29 g, 1.0 mmol) in methanol (20 cm^3) were mixed and stirred at room temperature. The resulting $PbSO_4$ was separated by filtration, and the filtrate was evaporated to dryness. The residue was dissolved in methanol (20 cm^3), and the solution was diffused with ether to give brown microcrystals. They were separated, washed successively with an ether–methanol (1:1 in volume) mixture and then ether, and dried in air. Yield: 0.71 g (87%). Anal. Calcd for $C_{25}H_{35}Cl_2CuN_5O_{13}Zn$: C, 36.92; H, 4.33; N, 8.61; Cu, 7.81; Zn, 8.04. Found: C, 36.83; H, 4.19; N, 8.45; Cu, 7.78; Zn, 7.83. μ_{eff}: 1.83 μ_B at 290 K. UV–vis data [λ/nm (ϵ/M^{-1} cm^{-1})] in acetonitrile: 369 (13 300), 529 (150). Selected IR data [ν/cm^{-1}] using KBr disks: 3350, 1645, 1640, 1105, 1080.

X-ray Structure Analyses of [CuPb(L1)](AcO)(BPh$_4$)·DMF (1c) and [CuMn(L1)](OAc)(BPh$_4$) (3c). Diffraction data were obtained on a Rigaku Denki AFC-4 four-circle diffractometer, using graphite-monochromatized Mo Kα radiation at 20 ± 1 °C. Pertinent crystallographic parameters are summarized in Table I. Three standard reflections were monitored every 100 measurements and showed no systematic decrease in intensity. Reflection data were corrected for Lorentz and polarization factors. Corrections for absorption effects were not made.

The structures were solved by the standard heavy-atom method and refined by block-diagonal least-squares calculations. Reliability factors are defined as $R = \Sigma(|F_o|-|F_c|)/\Sigma|F_o|$ and $R' = [\Sigma w(|F_o|-|F_c|)^2/\Sigma w|F_o|^2]^{1/2}$, where weights were taken as $w = 1$ for **1c** and $w = 1/|F_o|$ for **3c**. The contributions for hydrogen atoms bound to carbons were introduced in the calculated positions. These hydrogen atoms were included in the structure factor calculation but not refined. The atomic scattering factors were taken from ref 24. All computations were carried out on a FACOM M 780 computer at the Computer Center of Kyushu University using the UNICS III program.[25] The final atomic coordinates of **1c** and **3c** are given in Tables II and III, respectively.

Table I. Crystallographic Data for [CuPb(L1)](AcO)(BPh$_4$)·DMF (**1c**) and [CuMn(L1)](AcO)(BPh$_4$) (**3c**)

formula	$C_{53}H_{58}BCuN_6O_5Pb$	$C_{50}H_{50}BCuMnN_5O_4$
fw	1140.6	914.273
cryst size	0.2 × 0.2 × 0.3	0.3 × 0.3 × 0.3
cryst system	monoclinic	monoclinic
space group	$P2_1/n$	$P2_1/n$
a, Å	18.890(3)	17.508(8)
b, Å	19.968(3)	15.539(5)
c, Å	12.704(2)	16.515(5)
β, deg	91.61(1)	106.30(3)
V, Å^3	4790(1)	4312(3)
Z	4	4
λ(Mo Kα), Å	0.710 69	0.710 69
D_m, g cm^{-3}	1.530	1.401
D_x, g cm^{-3}	1.536	1.408
μ, cm^{-1}	40.3	8.25
no. of reflcns with $\lvert F_o\rvert \geq 3\sigma(F_o)$	4945	2935
F(000)	2296	1904
R,[a] %	6.97	6.89
R_w,[b] %	8.63[c]	5.63[d]

[a] $R = \Sigma\lvert\lvert F_o\rvert - \lvert F_c\rvert\rvert/\Sigma\lvert F_o\rvert$. [b] $R_w = \{\Sigma[w(\lvert F_o\rvert - \lvert F_c\rvert)^2]/\Sigma[w\lvert F_o\rvert^2]\}^{1/2}$. [c] $w = 1$. [d] $w = 1/\lvert F_o\rvert$.

Results and Discussion

Macrocyclic CuPb Complexes. The stepwise template reaction using Cu(II) and Pb(II) ions at the different stages of cyclization[21,22] was successfully applied to the synthesis of the macrocycles L1–L4, which were isolated as CuPb dinuclear complexes in good yields.

The structure of [CuPb(L1)](AcO)(Bph$_4$)·DMF (**1c**) was determined by single-crystal X-ray crystallography. The crystal

(24) *International Tables for X-Ray Crystallography*; Ibers, J. A., Hamilton, W. C., Eds.; Kynoch Press: Birmingham, U.K., 1974; Vol. 4.
(25) Sakurai, T.; Kobayashi, K. *Rikagaku Kennkyusho Houkoku* **1979**, *55*, 69 (Japanese).

Table II. Final Atomic Coordinates (×10⁴) and B_{eq} (Å²) Values of **1c**

atom	x	y	z	B_{eq}[a]	atom	x	y	z	B_{eq}[a]
Pb	639.7(3)	−17.5(4)	3347.5(5)	3.2	O(4)	851(8)	−993(10)	4405(16)	8.9
Cu	−409(1)	−321(1)	1007(1)	2.4	C(25)	351(11)	−1146(12)	4961(17)	5.9
O(1)	27(5)	505(5)	1396(8)	2.8	C(26)	437(17)	−1744(18)	5558(28)	11.8
O(2)	357(5)	−773(5)	1706(8)	2.5	B	−3316(1)	839(10)	2862(15)	3.3
N(1)	−1215(6)	101(7)	292(8)	2.6	C(27)	−4082(8)	413(8)	2944(12)	2.8
N(2)	−895(6)	−1139(6)	659(9)	2.3	C(28)	−4634(9)	490(10)	2205(15)	4.2
N(3)	1733(6)	−624(7)	2621(9)	2.8	C(29)	−5261(10)	110(12)	2248(18)	5.6
N(4)	1758(7)	325(7)	4327(9)	3.1	C(30)	−5340(9)	−343(10)	3037(17)	4.8
N(5)	1168(7)	1165(6)	2619(10)	2.9	C(31)	−4824(9)	−408(10)	3800(15)	4.4
C(1)	−1628(8)	−350(8)	−316(12)	2.8	C(32)	−4216(8)	−31(11)	3730(13)	3.8
C(2)	−1634(8)	−1001(9)	206(11)	2.7	C(33)	−2655(9)	285(9)	2919(12)	3.1
C(3)	−679(8)	−1732(8)	773(12)	2.6	C(34)	−2724(10)	−408(10)	2821(15)	4.3
C(4)	17(8)	−1900(7)	1179(11)	2.6	C(35)	−2148(11)	−844(10)	2870(15)	4.6
C(5)	203(9)	−2567(9)	1120(14)	3.5	C(36)	−1478(9)	−587(11)	3037(13)	4.3
C(6)	875(9)	−2812(9)	1446(15)	4.0	C(37)	−1397(9)	73(11)	3155(13)	4.3
C(7)	1079(10)	−3546(9)	1356(19)	5.3	C(38)	−1960(8)	523(9)	3070(14)	3.4
C(8)	1353(9)	−2333(9)	1822(15)	3.9	C(39)	−3232(9)	1366(8)	3871(15)	3.5
C(9)	1197(8)	−1639(8)	1961(12)	3.0	C(40)	−2707(10)	1866(10)	3803(18)	5.0
C(10)	506(8)	−1408(8)	1617(11)	2.7	C(41)	−2565(11)	2270(11)	4676(21)	6.1
C(11)	1773(8)	−1236(9)	2326(12)	3.2	C(42)	−2922(13)	2221(11)	5604(20)	6.5
C(12)	2407(8)	−316(9)	2975(13)	3.4	C(43)	−3458(11)	1744(10)	5622(16)	5.2
C(13)	2356(9)	−116(9)	4114(13)	3.7	C(44)	−3607(10)	1340(9)	4786(15)	4.0
C(14)	1878(10)	1033(10)	4271(13)	4.2	C(45)	−3330(8)	1225(9)	1740(15)	3.8
C(15)	1868(9)	1311(9)	3109(14)	3.7	C(46)	−3507(12)	1882(11)	1604(21)	6.4
C(16)	825(9)	1668(8)	2335(12)	3.1	C(47)	−3554(14)	2174(13)	580(27)	9.7
C(17)	88(9)	1670(8)	1812(14)	3.4	C(48)	−3418(13)	1768(17)	−320(21)	9.1
C(18)	−262(11)	2296(9)	1833(16)	4.7	C(49)	−3244(10)	1135(13)	−212(15)	5.7
C(19)	−947(10)	2388(9)	1499(15)	4.1	C(50)	−3206(10)	872(13)	809(17)	6.1
C(20)	−1294(12)	3047(11)	1611(21)	6.5	O(D)	3150(12)	1212(16)	995(18)	14.0
C(21)	−1266(9)	1852(9)	1068(15)	3.9	N(D)	4066(13)	1315(13)	130(24)	11.9
C(22)	−965(8)	1232(8)	962(12)	2.8	C(D1)	4236(29)	1969(34)	772(50)	22.4
C(23)	−265(8)	1097(8)	1416(12)	2.8	C(D2)	4682(25)	1358(38)	−395(47)	25.0
C(24)	−1361(8)	729(8)	424(11)	2.9	C(D3)	3557(23)	989(21)	134(46)	18.8
O(3)	−180(8)	−793(9)	5013(14)	7.8					

Table III. Final Atomic Coordinates (×10⁴) and B_{eq} (Å²) Values of **3c**

atom	x	y	z	B_{eq}[a]	atom	x	y	z	B_{eq}[a]
Cu	57(1)	3628(1)	1534(1)	3.2	C(23)	1178(6)	76(6)	1260(8)	4.7
Mn	1199(1)	2069(1)	1606(1)	2.7	C(24)	−103(6)	539(6)	1135(6)	3.2
O(1)	−73(4)	2388(4)	1458(4)	3.4	O(3)	1546(4)	2529(4)	2831(4)	3.6
O(2)	966(4)	3439(3)	1114(4)	3.1	O(4)	809(4)	3692(5)	2830(4)	4.9
N(1)	−952(5)	3802(5)	1774(5)	3.5	C(25)	1358(6)	3190(6)	3182(7)	3.8
N(2)	0(5)	4859(4)	1313(5)	3.2	C(26)	1807(7)	3383(7)	4072(7)	5.3
N(3)	2080(5)	2254(5)	878(5)	3.6	B	−459(7)	−2006(8)	2823(8)	3.2
N(4)	2222(5)	1008(5)	2139(5)	3.5	C(27)	41(6)	−2127(6)	2106(6)	3.0
N(5)	604(5)	797(5)	1234(5)	3.1	C(28)	−282(6)	−2186(7)	1264(6)	3.8
C(1)	−2960(6)	521(7)	1025(7)	4.1	C(29)	174(7)	−2243(6)	691(7)	4.2
C(2)	−2201(6)	1018(6)	1110(7)	3.5	C(30)	984(7)	−2230(7)	974(7)	4.3
C(3)	−2158(6)	1874(7)	1327(7)	4.2	C(31)	1325(6)	−2181(6)	1803(7)	3.8
C(4)	−1455(6)	2361(6)	1458(6)	3.0	C(32)	877(6)	−2120(6)	2375(6)	3.1
C(5)	−746(6)	1968(6)	1362(6)	2.8	C(33)	−111(6)	−2671(6)	3621(7)	3.1
C(6)	−799(6)	1088(6)	1162(6)	2.9	C(34)	168(6)	−3500(6)	3491(7)	3.7
C(7)	−1505(6)	627(6)	1055(7)	3.6	C(35)	396(6)	−4108(6)	4145(8)	4.4
C(8)	−1503(6)	3244(6)	1717(6)	3.7	C(36)	346(7)	−3917(7)	4933(7)	4.9
C(9)	−1023(7)	4707(7)	2024(7)	4.1	C(37)	86(7)	−3118(7)	5083(7)	5.3
C(10)	−730(6)	5258(6)	1409(7)	3.6	C(38)	−139(6)	−2508(6)	4441(6)	3.8
C(11)	528(6)	5301(5)	1105(7)	3.5	C(39)	−1394(6)	−2265(6)	2345(6)	3.3
C(12)	1240(6)	4952(6)	946(7)	3.4	C(40)	−1670(6)	−3125(6)	2285(7)	3.3
C(13)	1748(6)	5565(6)	739(7)	3.7	C(41)	−2432(7)	−3353(7)	1824(7)	4.5
C(14)	2430(6)	5328(6)	527(7)	3.6	C(42)	−2951(6)	−2745(7)	1370(7)	4.5
C(15)	2963(7)	6007(7)	309(8)	5.1	C(43)	−2702(6)	−1904(7)	1430(8)	4.9
C(16)	2608(6)	4466(6)	523(7)	3.5	C(44)	−1935(6)	−1660(6)	1913(7)	4.1
C(17)	2116(6)	3816(6)	719(6)	3.1	C(45)	−412(6)	−1012(6)	3146(6)	2.8
C(18)	1420(6)	4050(6)	944(6)	3.0	C(46)	−913(6)	−686(7)	3598(8)	4.3
C(19)	2392(6)	2933(6)	654(6)	3.5	C(47)	−887(8)	143(7)	3890(8)	5.6
C(20)	2514(6)	1449(6)	805(8)	4.5	C(48)	−333(7)	718(6)	3737(7)	4.7
C(21)	2830(6)	1062(6)	1671(8)	4.1	C(49)	148(7)	431(6)	3270(8)	5.2
C(22)	1843(6)	152(6)	2054(8)	5.1	C(50)	118(6)	−405(6)	2985(7)	3.8

[a] $B_{eq} = {}^4/_3[a^2B_{11}+b^2B_{22}+c^2B_{33}+2ab(\cos\gamma)B_{12} + 2ac(\cos\beta)B_{13}+2bc(\cos\alpha)B_{23}]$.

is composed of the dimeric complex cation $\{CuPb(L1)(OAc)\}_2^{2+}$, tetraphenylborate anions, and DMF molecules which are captured in the crystal lattice. The ORTEP view of the complex cation is shown in Figures 1 and 2. The relevant bond distances and angles are summarized in Table IV.

The Cu(II) ion is located at the 4-coordination site of the macrocycle L1 and assumes a nearly planar environment with N(1), N(2), O(1), and O(2). The deviation of the Cu from the least-squares plane defined by the donor atoms is less than 0.03 Å. The Cu–O and Cu–N bond distances fall in the range of

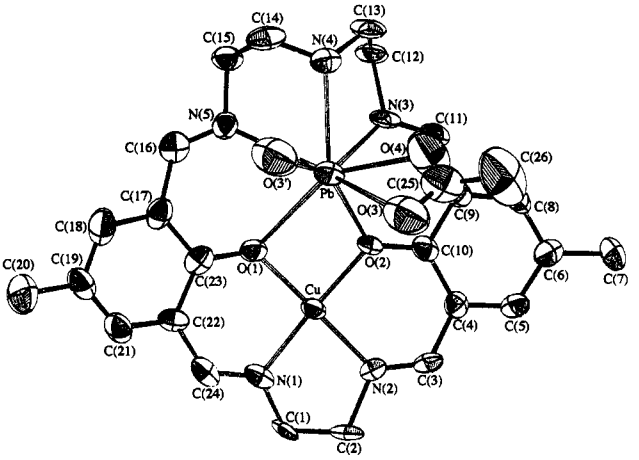

Figure 1. ORTEP view of the $\{CuPb(L1)(AcO)\}^+$ part of **1c**.

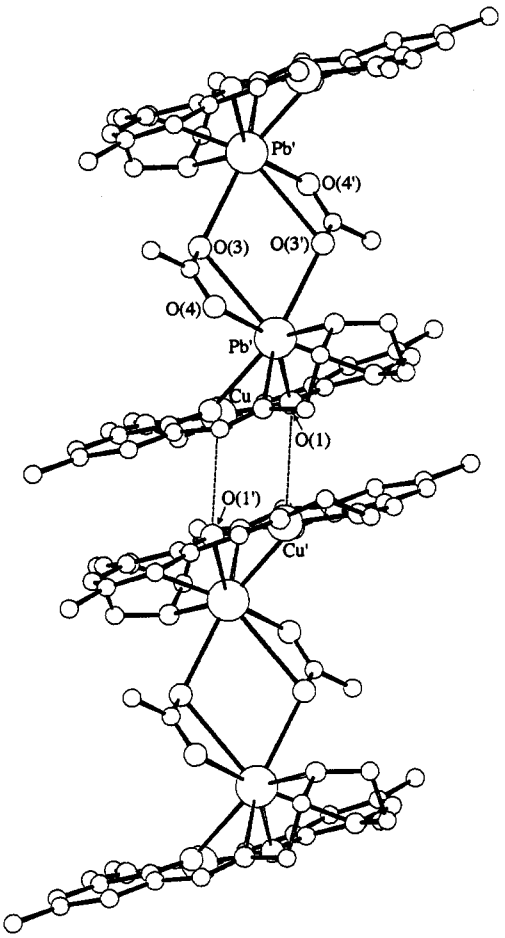

Figure 2. Intermolecular interaction mode of $\{CuPb(L1)(AcO)\}^+$.

1.90(1)–1.94(1) Å and are slightly elongated relative to those of [*N*,*N*′-bis(salicylidene)ethylenediaminato]copper(II) [Cu(salen)].[26]

The lead(II) ion is bound at the 5-coordination site and is eight-coordinated to N(3), N(4), N(5), O(1), and O(2) of the macrocycle and O(3), O(4), and O(3′) of the acetate groups. The acetate group coordinates to Pb through its O(3) and O(4) and to Pb′ through O(3), acting as the bridge between Pb and Pb′ (see Figure 2). The Pb(II) ion cannot reside within the cavity of the macrocycle because of its large ionic radius and deviates by 1.60 Å from the least-squares plane defined by N(3), N(5), O(1), and O(2). The Pb–N(4) distance (2.52(1) Å) is the shortest among the bonds to the macrocycle probably for steric reasons, whereas the Pb–O(1) bond is significantly elongated (2.90(1) Å). It is noted that the acetate group strongly coordinates to the Pb(II) ion (Pb–O(4) = 2.39(2) Å); the bridging Pb–O(3) and Pb–O(3′) bonds are longer (3.08(2) and 2.80(2) Å, respectively). The Cu–Pb separation, bridged by O(1) and O(2), is 3.577(2) Å, and the Pb- -Pb′ separation is 4.904(1) Å.

Table IV. Relevant Bond Distances (Å) and Angles (deg) of **1c**

Bond Distances					
Cu–O(1)	1.90(1)	Cu–O(2)	1.90(1)	Cu–N(1)	1.94(1)
Cu–N(2)	1.92(1)	Pb–O(1)	2.90(1)	Pb–O(2)	2.62(1)
Pb–N(3)	2.59(1)	Pb–N(4)	2.52(1)	Pb–N(5)	2.74(1)
Pb–O(3)	3.08(2)	Pb–O(4)	2.39(2)	Cu–Pb	3.577(2)
Pb–Pb′	4.904(1)	Cu–Cu′	3.287(3)	Cu–O(1′)	3.18(1)
Pb–O(3′)	2.80(2)				

Bond Angles			
O(1)–Cu–O(2)	88.4(4)	O(1)–Cu–N(1)	94.2(5)
O(2)–Cu–N(2)	93.2(5)	N(1)–Cu–N(2)	84.1(5)
Cu–O(1)–Pb	94.0(4)	Cu–O(2)–Pb	103.5(4)
O(1)–Pb–O(2)	57.2(3)	O(1)–Pb–N(5)	62.7(3)
O(1)–Pb–O(3)	124.9(4)	O(1)–Pb–O(3′)	107.7(4)
O(2)–Pb–N(3)	66.0(3)	O(2)–Pb–O(3)	99.4(4)
O(2)–Pb–O(4)	90.3(5)	N(3)–Pb–N(4)	68.6(4)
N(3)–Pb–N(5)	88.9(4)	N(3)–Pb–O(3)	115.6(4)
N(3)–Pb–O(4)	72.4(5)	N(4)–Pb–N(5)	67.9(4)
N(4)–Pb–O(3)	103.2(4)	N(4)–Pb–O(4)	79.6(5)
N(4)–Pb–O(3′)	75.4(4)	N(5)–Pb–O(3′)	82.9(5)
O(3)–Pb–O(4)	44.2(5)	O(3)–Pb–O(3′)	66.8(5)
O(4)–Pb–O(3′)	96.0(6)		

In the crystal, the dimeric cations further interact through out-of-plane bonding between the CuN_2O_2 entities (see Figure 2). That is, O(1) coordinates to the axial site of Cu′ of the neighboring molecule and in turn O(1′) coordinates to the axial site of Cu, affording a column along the *a* axis of the crystal. The Cu–O(1′) separation is 3.18(1) Å, and the Cu- -Cu′ separation is 3.287(3) Å. Such an out-of-plane bonding is commonly seen for metal complexes of salen-like ligands.[27,28]

The magnetic moment of **1c** is 1.93 μ_B at room temperature. Other CuPb complexes also show a magnetic moment falling in the range 1.90–1.98 μ_B. The relatively large magnetic moments of these complexes suggest a ferromagnetic interaction between a pair of copper(II) ions through the out-of-plane bonding.[29] The IR spectrum of **1c** shows the antisymmetric and symmetric ν(COO) vibrations of the acetate group at 1542 and 1438 cm^{-1}, respectively. Such a small separation of the vibration modes is commonly seen for bridging carboxylate groups.[30] In the perchlorate salts, **1a** and **2**, the perchlorate ion must be coordinated as a uni- or bidentate ligand as judged from the split ν_3 band[31] (see Experimental Section). On the other hand, we could not decide, on the basis of IR spectra, if the nitrate group of **1b** is associated with coordination to the Pb. All the CuPb complexes show a d–d band maximum at 546–586 nm in acetonitrile, suggesting an essentially planar configuration about each Cu(II) ion.[12,32,33]

[CuM(L1)]XY Complexes. The conversion of the $Cu^{II}Pb^{II}$ complexes into the $Cu^{II}M^{II}$ complexes by transmetalation was studied using the CuPb complexes of L1, **1a–c**, as the precursor complexes, and a series of CuM complexes (M = Mn, Fe, Co, Ni, Cu, Zn) were obtained in good yields when stoichiometric amounts of a precursor complex and a metal(II) sulfate were reacted in an appropriate solvent. In this reaction, Pb(II) ion was deposited as $PbSO_4$ and each CuM complex was isolated as the same salt with the XY anion as the respective precursor

(26) Baker, E. N.; Hall, D.; Waters, T. N. *J. Chem. Soc. A* **1970**, 400, 406.

(27) Hall, D.; Waters, T. N. *J. Chem. Soc.* **1960**, 2644.

(28) Calligaris, M.; Nardin, G.; Randaccio, L. *Coord. Chem. Rev.* **1972**, *7*, 385. Hobday, M. D.; Smith, T. D. *Ibid.* **1972–1973**, *9*, 311.

(29) Carlisle, G. O.; Hatfield, W. E. *Inorg. Nucl. Chem. Lett.* **1970**, *6*, 633.

(30) Deacon, G. B.; Phillips, R. J. *Coord. Chem. Rev.* **1980**, *23*, 227.

(31) Nakamoto, K. *Infrared Spectra of Inorganic and Coordination Compounds*, 2nd ed.; John Wiley & Sons: New York, 1970; p 175.

(32) Gruber, S. J.; Harris, C. M.; Sinn, E. *Inorg. Nucl. Chem. Lett.* **1968**, *4*, 107.

(33) Dawning, R. S.; Urbach, F. L. *J. Am. Chem. Soc.* **1969**, *91*, 5977. Crawford, S. M. *Spectrochim. Acta* **1963**, *19*, 255.

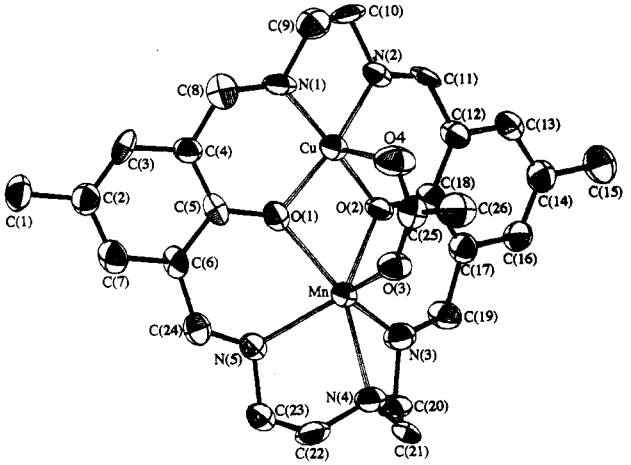

Figure 3. ORTEP view of the $\{CuMn(L1)(AcO)\}^+$ part of **3c**.

Table V. Relevant Bond Distances (Å) and Angles (deg) of **3c**

Bond Distances					
Cu–Mn	3.122(2)	Cu–O(1)	1.940(6)	Cu–O(2)	1.928(8)
Cu–N(1)	1.936(9)	Cu–N(2)	1.944(7)	Cu–O(4)	2.178(7)
Mn–O(1)	2.226(7)	Mn–O(2)	2.274(6)	Mn–N(3)	2.23(1)
Mn–N(4)	2.412(8)	Mn–N(5)	2.238(7)	Mn–O(3)	2.070(7)

Bond Angles			
O(1)–Cu–O(2)	85.3(3)	O(1)–Cu–N(1)	93.2(3)
O(1)–Cu–O(4)	97.9(3)	O(2)–Cu–N(2)	95.0(3)
O(2)–Cu–O(4)	91.6(3)	N(1)–Cu–N(2)	84.2(4)
N(1)–Cu–O(4)	97.3(3)	N(2)–Cu–O(4)	97.2(3)
O(1)–Mn–O(2)	71.3(2)	O(1)–Mn–N(5)	78.0(3)
O(1)–Mn–O(3)	92.4(3)	O(2)–Mn–N(3)	76.6(3)
O(2)–Mn–O(3)	90.0(2)	N(3)–Mn–N(4)	74.3(3)
N(3)–Mn–N(5)	107.8(3)	N(3)–Mn–O(3)	115.2(3)
N(4)–Mn–N(5)	74.8(3)	N(4)–Mn–O(3)	84.0(3)
N(5)–Mn–O(3)	124.0(3)	Mn–O(1)–Cu	96.8(3)
Mn–O(2)–Cu	95.6(3)		

complex. The $Cu^{II}M^{II}$ complexes, except for **4** (CuFe), are stable against molecular oxygen even in solution.

The crystal structure of $[CuM(L1)](AcO)(Bph_4)$ (**3c**) was determined by X-ray crystallography. The crystal is comprised of the complex cation, $\{CuMn(L1)(AcO)\}^+$, and tetraphenylborate ion. The ORTEP view of the cation is shown in Figure 3 together with the numbering scheme. The relevant bond distances and angles are given in Table V.

The Cu(II) and Mn(II) ions are bridged by the phenolic oxygens, O(1) and O(2), and by the acetate group. The Cu is in the same 4-coordination site as found in the precursor CuPb complex and assumes a nearly square-pyramidal geometry with N(1), N(2), O(1), and O(2) of the macrocycle L1 as the basal plane and O(4) of the bridging acetate group as the apex. The axial Cu–O(4) bond length is 2.178(7) Å and is longer than the basal bonds (1.928(8)–1.944(7) Å). The Cu deviates by 0.20 Å from the basal least-squares plane toward O(4).

The Mn is bound at the 5-coordination site and assumes a six-coordinate structure with O(1), O(2), N(3), N(4), and N(5) of the macrocycle and O(3) of the bridging acetate group. The donor atoms, O(1), O(2), N(3), and N(5), are nearly coplanar, and Mn deviates by 0.74 Å from the least-squares plane toward O(3). The amine nitrogen, N(4), is deviated by 1.90 Å from the least-squares plane and makes a bond to the Mn on the same side as O(3) with respect to the least-squares plane. Thus, the environment about the Mn is severely distorted from that of a regular octahedron. It should be emphasized that the bond lengths between the Mn and the donor atoms, except for Mn–O(3) (2.070(7) Å), are significantly elongated relative to common Mn(II)–N and Mn(II)–O bonds.[34-36]

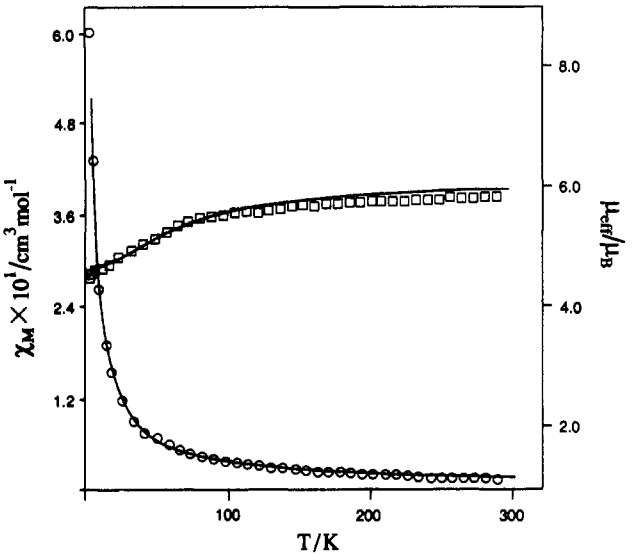

Figure 4. Temperature variations of magnetic susceptibility (○) and effective magnetic moment (□) per CuMn of **3c**. Solid lines are drawn on the basis of eq 1 using $J = -13.5\ cm^{-1}$, $g_{Cu} = 2.08$, $g_{Mn} = 2.00$, $\Theta = -1.1$ K, and $N\alpha = 60 \times 10^{-6}\ cm^3\ mol^{-1}$.

The least-squares plane defined by N(1), N(2), O(1), and O(2) and the plane defined by N(3), N(5), O(1), and O(2) are bent at the O(1)- -O(2) edge due to the bridge of the acetate group between the Cu and Mn ions. The dihedral angle between the two least-squares planes is 4.2°. The Cu- -Mn separation is 3.122(2) Å.

Selected IR bands of the CuM complexes are given in the Experimental Section. The $\nu_{as}(COO)$ and $\nu_s(COO)$ modes of the bridging acetate group in **3c** are seen at 1575 and 1440 cm^{-1}, respectively. The perchlorate anion in **3c**, **4**, **5a**, **6**, and **8** may be coordinated to the M(II) ion, but the anion must be free from coordination in **7** since no splitting of the perchlorate ν_3 band is detected.

Magnetic properties of the CuM complexes were studied in the temperature range 4.2–300 K. The room-temperature magnetic moments of the CuMn (**3a–c**), CuFe (**4**), CuCo (**5a,b**), CuNi (**6**), and Cu_2 (**7**) complexes are lower than the respective spin-only value for magnetically diluted Cu(II)–M(II) ($S_{Cu} = {}^1/_2$, $S_{Mn} = {}^5/_2$, $S_{Fe} = 2$, $S_{Co} = {}^3/_2$, $S_{Ni} = 1$) and decrease with decreasing temperature. Such magnetic behavior is characteristic of an intramolecular antiferromagnetic spin-exchange interaction.

The temperature variations of magnetic susceptibility and magnetic moment of **3c** are shown in Figure 4. The magnetic moment, μ_{eff} per CuMn, decreases with decreasing temperature and converges to ca. 4.9 μ_B near liquid-helium temperature. This moment is close to the spin-only value for $S_T = 2$ arising from the antiferromagnetic coupling of $S_{Cu} = {}^1/_2$ and $S_{Mn} = {}^5/_2$. The magnetic analysis was carried out using the magnetic susceptibility eq 1 for the $(S_1 = {}^1/_2) - (S_2 = {}^5/_2)$ system based on the isotropic

$$\chi_M = \frac{N\beta^2}{k(T-\Theta)} \frac{28g_3^2 + 10g_2^2 \exp(-6J/kT)}{7 + 5\exp(-6J/kT)} + N\alpha \quad (1)$$

Heisenberg model $\mathcal{H} = -2JS_1S_2$ and including the Weiss term, where χ_M is the magnetic susceptibility per CuMn, N is Avogadro's number, β is the Bohr magneton, k is the Boltzmann constant, J is the exchange integral, T is the absolute temperature, and $N\alpha$ is the temperature-independent paramagnetism. The g factors for the total spin-states $S_T = 2$ and 3, g_2 and g_3, are derived arithmetically[37,38] as $g_2 = (7g_{Mn} - g_{Cu})/6$ and $g_3 = (5g_{Mn} + g_{Cu})/$

(34) Mabad, B.; Cassoux, P.; Tuchagues, J.-P.; Hendrickson, D. N. *Inorg. Chem.* **1986**, *25*, 1420.
(35) Takahashi, K.; Nishida, Y.; Kida, S. *Inorg. Chim. Acta* **1983**, *77*, L185.
(36) Kessissoglou, D. P.; Butler, W. M.; Pecoraro, V. L. *Inorg. Chem.* **1987**, *26*, 495.
(37) Chao, C. C. *J. Magn. Reson.* **1973**, *10*, 1.
(38) Scaringe, R. P.; Hodgson, D. J.; Hatfield, W. E. *Mol. Phys.* **1978**, *35*, 701.

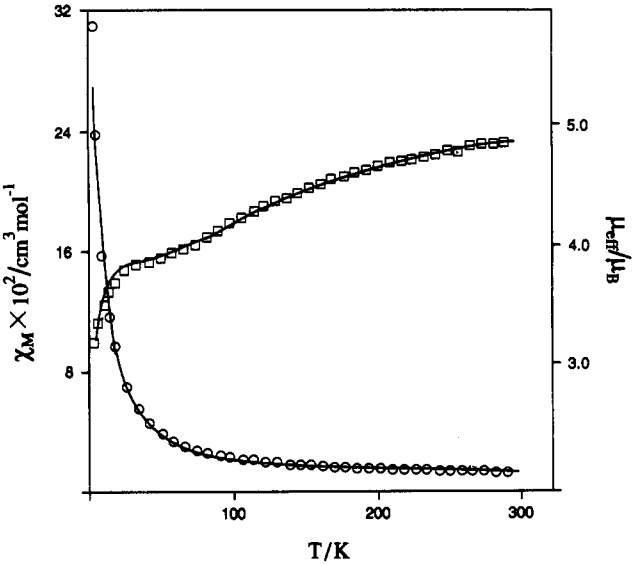

Figure 5. Temperature variations of magnetic susceptibility (○) and effective magnetic moment (□) per CuFe of **4**. Solid lines are drawn on the basis of the equation in ref 14e using $J = -37$ cm^{-1}, $g_{av} = 2.06$, and $D = -1.08$ cm^{-1}.

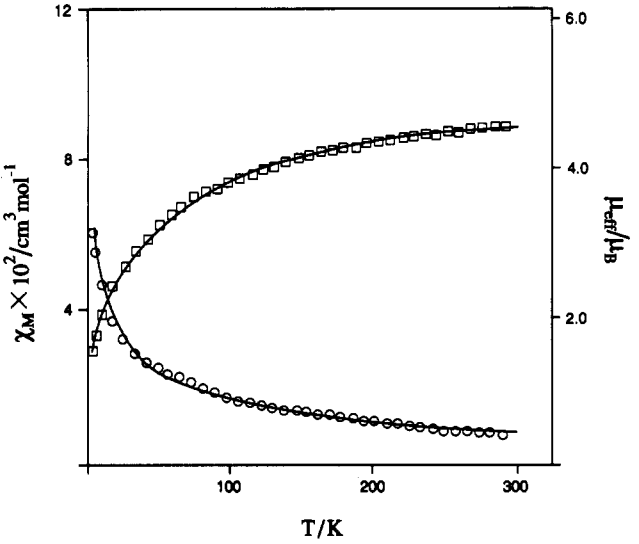

Figure 6. Temperature variations of magnetic susceptibility (○) and effective magnetic moment (□) per CuCo of **5a**. Solid lines are drawn on the basis of eq 2 using $J = -21.5$ cm^{-1}, $g_{Cu} = 2.10$, $g_{Co} = 2.25$, and $\Theta = -14.9$ K.

6. As indicated by the solid lines in Figure 4, a tolerable magnetic simulation for **3c** is obtained with eq 1 using $J = -13.5$ cm^{-1}, $g_{Cu} = 2.08$, $g_{Mn} = 2.00$, $\Theta = -0.5$ K, and $N\alpha = 60 \times 10^{-6}$ cm^3 mol^{-1}. The disrepancy factor defined as $R(\chi) = [\Sigma(\chi_{obsd}-\chi_{calcd})^2/\Sigma(\chi_{obsd})^2]^{1/2}$ was 5.8×10^{-2}. The zero-field splitting effect of Mn(II) was presumed to be the origin for a slight disagreement in the fitting, but our magnetic analyses by taking into account this effect[14e] could not improve the fitting. It appears that some other factors such as a structural change with temperature contribute to the overall magnetic behavior of **3c**. For **3a,b** a better magnetic simulation was obtained using eq 1 with $R(\chi) = 3.1 \times 10^{-2}$ and 8.5×10^{-3}, respectively. The exchange integrals evaluated for **3a,b** were -20.0 and -19.0 cm^{-1}, respectively. The exchange integrals of the present CuMn complexes are small in absolute value compared with the values ($-J = 30$–36 cm^{-1}) found for the CuMn complexes of macrocycle I ($m = n = 3$)[14e] and *N,N'*-alkylbis(3-carboxysalicylideneaminates).[39,40] The reduced antiferromagnetic spin-exchange in the present CuMn complexes may be attributed to the distorted configuration about the Mn(II) as proved for **3c**.

The cryomagnetic property of the CuFe complex **4** is given in Figure 5. With decreasing temperature, the moment decreases to a plateau around 50–75 K and then decreases further below 50 K. The plateau moment is ca. 3.9 μ_B, which corresponds to the spin-only value for $S = {}^3/_2$ resulting from antiferromagnetic spin-coupling of $S_{Cu} = {}^1/_2$ and $S_{Fe} = 2$. The magnetic behavior demonstrates that the antiferromagnetic spin-coupling between the Cu(II) and Fe(II) ions is dominant, but a second, weaker effect operates to cause a reduction in the magnetic moment below 50 K. The most plausible second effect is zero-field splitting associated with the Fe(II) ion.[14e] The magnetic susceptibility equation for the Cu(II)–Fe(II) system based on the Hamiltonian including zero-field splitting term, $\mathcal{H} = -2JS_1S_2 - DS_z^2$, has been derived by Lambert et al.[14e] We have adopted their magnetic expression to analyze the magnetism of **4** and obtained a fairly good simulation as indicated in Figure 5 using $J = -37$ cm^{-1}, $g_{av} = 2.06$, and $D = -1.08$ cm^{-1}. The discrepancy factor was 4.12×10^{-2}. The temperature-independent paramagnetism, $N\alpha$, is assumed to be zero in the simulation. The exchange integral (-37 cm^{-1}) is again smaller in absolute value than the -71 cm^{-1} found for the diphenoxo-bridged $Cu^{II}Fe^{II}$ complex of macrocycle I ($m = n = 3$).[14e]

The χ_M vs T and μ_{eff} vs T curves for **5a** are given in Figure 6. The magnetic moments of the CuCo complexes **5a,b** are 4.57 and 4.74 μ_B, respectively, at room temperature and decrease monotonically to values of 1.47 and 1.37 μ_B, respectively, at liquid-helium temperature. The moments at liquid-helium temperature are much smaller than the spin-only value for $S_T = 1$ resulting from antiferromagnetic coupling between $S_{Cu} = {}^1/_2$ and $S_{Co} = {}^3/_2$. This fact suggests that the antiferromagnetic spin-exchange between the Cu(II) and Co(II) ions is dominant but some other factors significantly contribute to the magnetism of **5a,b**. Notably, the magnetic behaviors of these complexes resemble that of the previously reported CuCo complex of macrocycle I ($m = n = 3$).[14e] Magnetic simulations for the previous complex could be performed by taking into account the zero-field splitting of Co(II) ($D = -2.56$ cm^{-1}) and adding a very large Weiss parameter ($\Theta = -27.8$ K). In our magnetic analyses, the zero-field splitting term is neglected because its contribution to the overall magnetism seems to be smaller than the effect from the Weiss parameter. The magnetic susceptibility expression is given as

$$\chi_M = \frac{N\beta^2}{k(T-\Theta)} \frac{10g_2^2 + 2g_1^2 \exp(-4J/kT)}{5 + 3\exp(-4J/kT)} \qquad (2)$$

where $g_1 = (5g_{Co} - g_{Cu})/4$ and $g_2 = (3g_{Co} + g_{Cu})/4$. A tolerable best-fit is obtained with this equation using $J = -21.5$ cm^{-1}, $g_{Co} = 2.25$, $g_{Cu} = 2.10$, and $\Theta = -14.9$ K for **5a** as shown in Figure 6. The discrepancy factor was 3.8×10^{-2}. A similar fitting for **5b** gave the magnetic parameters of $J = -23.5$ cm^{-1}, $g_{Co} = 2.32$, $g_{Cu} = 2.10$, and $\Theta = -7.0$ K with $R(\chi) = 1.2 \times 10^{-1}$.

The cryomagnetic property of the CuNi complex **6** is shown in Figure 7. The magnetic analysis of this complex was made using expression 3 based on the Heisenberg model:

$$\chi_M = \frac{N\beta^2}{4k(T-\Theta)} \frac{10g_{3/2}^2 + g_{1/2}^2 \exp(-3J/kT)}{2 + \exp(-3J/kT)} + N\alpha \qquad (3)$$

Here $g_{1/2} = (4g_{Ni} - g_{Cu})/3$ and $g_{3/2} = (2g_{Ni} + g_{Cu})/3$. A fairly good magnetic simulation is obtained based on eq 3 using $J = -110$ cm^{-1}, $g_{Cu} = 2.10$, $g_{Ni} = 2.12$, $\Theta = -0.5$ K, and $N\alpha = 280 \times 10^{-6}$ cm^3 mol^{-1}. The discrepancy factor was 8.7×10^{-3}. A slight deviation is observed between the experimental and theoretical values in the ranges 100–190 and 250–300 K. Similar deviations in best-fitting have been observed in the related CuNi complex of macrocycle I ($m = n = 3$).[14e]

The cryomagnetic properties of the Cu_2 complex **7** are shown in Figure 8. The magnetic analysis for this complex was made

(39) Torihara, N.; Okawa, H.; Kida, S. *Chem. Lett.* **1978**, 185.
(40) Kahn, O.; Tola, P.; Coudanne, H. *Chem. Phys.* **1979**, *42*, 355. Tola, P.; Kahn, O.; Chauvel, C.; Coudanne, H. *Nouv. J. Chim.* **1979**, *1*, 467.

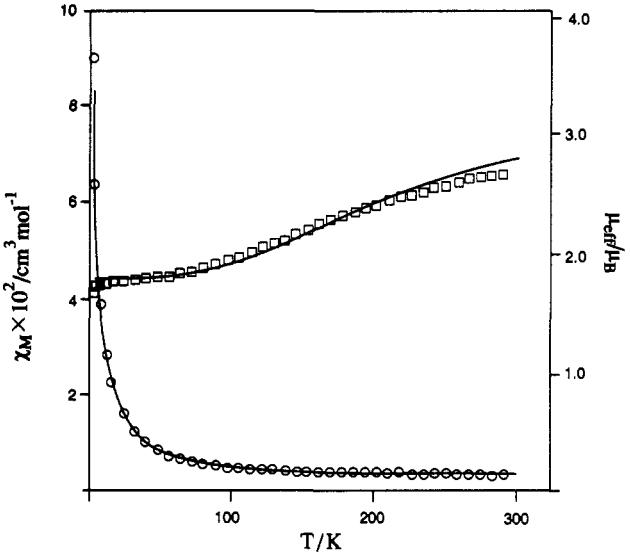

Figure 7. Temperature variations of magnetic susceptibility (○) and effective magnetic moment (□) per CuNi of **6**. Solid lines are drawn on the basis of eq 3 using $J = -110$ cm^{-1}, $g_{Cu} = 2.10$, $g_{Ni} = 2.12$, $\Theta = -0.5$ K, and $N\alpha = 280 \times 10^{-6}$ cm^3 mol^{-1}.

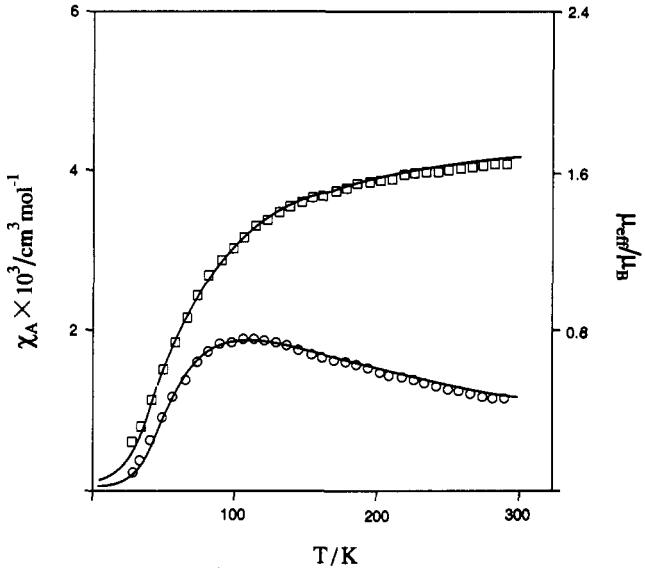

Figure 8. Temperature variations of magnetic susceptibility (○) and effective magnetic moment (□) per Cu of **7**. Solid lines are drawn on the basis of eq 4 using $J = -110$ cm^{-1}, $g = 2.08$, and $N\alpha = 60 \times 10^{-6}$ cm^3 mol^{-1}.

using the Bleaney–Bowers equation,[41]

$$\chi_A = \frac{Ng^2\beta^2}{kT}\frac{1}{3 + \exp(-2J/kT)} + N\alpha \qquad (4)$$

where χ_A is the magnetic susceptibility per one Cu. As seen in Figure 8, a good magnetic simulation is obtained using $J = -62$ cm^{-1}, $g = 2.08$, and $N\alpha = 60 \times 10^{-6}$ cm^3 mol^{-1}. The discrepancy factor was 2.8×10^{-2}. The observed antiferromagnetic spin-exchange is weak, reflecting the distorted configuration around the Cu(II) at the 5-coordination site of L1. The magnetic data for the CuM complexes are summarized in Table VI.

Electronic spectra of the CuM complexes as perchlorate salts measured in acetonitrile are given in Figures 9 and 10. Numerical data are given in the Experimental Section. Each complex shows an intense band at 366 ± 2 nm which is assigned to the intraligand π–π^* transition band associated with the C=N linkages.[42,43] In

(41) Bleaney, B.; Bowers, K. D. *Proc. R. Soc. London, Ser. A* **1952**, *214*, 451.
(42) Bosnich, B. *J. Am. Chem. Soc.* **1968**, *90*, 627.
(43) Downing, R. S.; Urbach, F. L. *J. Am. Chem. Soc.* **1969**, *91*, 5977.

Table VI. Magnetic Data for the [CuM(L1)]XY Complexes

	J/cm^{-1}	g_{Cu}	g_M	g_{av}	Θ/K	D/cm^{-1}	$10^6 N\alpha$/cm^3 mol^{-1}
3a	−20.0	2.10	2.00		−0.5		60
3b	−19.0	2.10	2.00		−0.1		60
3c	−13.5	2.08	2.00		−1.1		60
4	−37.0			2.06		−1.08	
5a	−21.5	2.10	2.25		−14.9		0
5b	−23.5	2.10	2.32		−7.0		0
6	−110	2.10	2.12		−0.5		280
7	−62.0	2.08					60

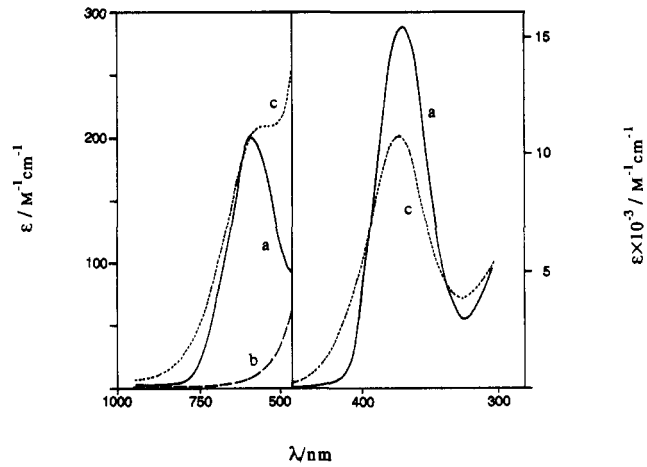

Figure 9. Electronic spectra of **3a** in acetonitrile (trace a), its one-electron reduced complex in DMSO (trace b), and one-electron oxidized complex in acetonitrile (trace c).

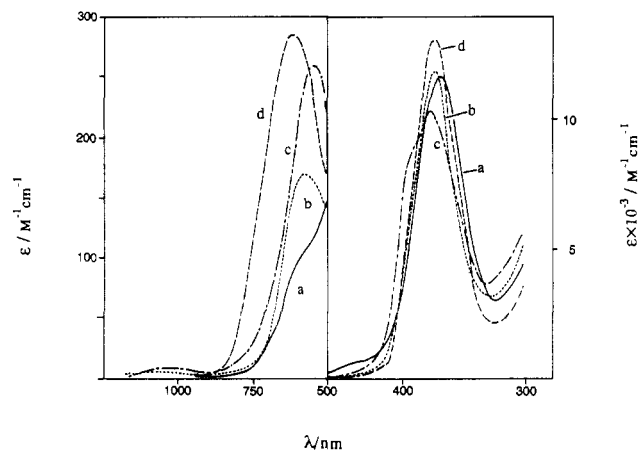

Figure 10. Electronic spectra of CuM complexes in acetonitrile: trace a, **4** (CuFe); trace b, **5a** (CuCo); trace c, **6** (CuNi); trace d, **7** (Cu_2). The extinction coefficient is given per CuM.

the case of the Cu_2 complex **7**, a splitting of the π–π^* band is seen. The d–d transition bands of the constituent metal ions appear in the region below 450 nm. The CuMn and CuZn complexes (**3a** and **8**) show one visible band due to the Cu(II) ion at 547 and 529 nm, respectively (see Figure 10). The other CuM complexes (**4**, **5a**, **6**, **7**) show superposed d–d transition bands from the Cu(II) and M(II) ions, but the d–d band of the Cu(II) ion is always well resolved because this band is stronger than the d–d band(s) of the M(II) ions. For the CuFe complex **4**, the band at 468 nm is ascribed to the d–d band of the Fe(II) ion. The Co(II) of **5a** shows a d–d band at 1115 nm, and the Ni(II) of **6** shows a d–d band at 1015 nm. In the spectrum of the Cu_2 complex **7**, the d–d bands of the two Cu(II) ions appear as a superposed band with a large extinction coefficient ($\epsilon = 290$ M^{-1} cm^{-1}) at 568 nm. The electronic spectral results indicate that the CuM complexes are stable and retain their discrete heterodinuclear structures in solution.

The electrochemical behavior of the CuM complexes as perchlorate salts was studied by means of cyclic voltammetry in

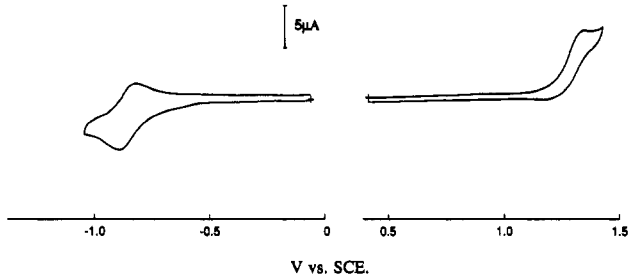

Figure 11. Cyclic voltammograms of **3a** (CuMn): glassy-carbon electrode, scan rate 80 mV s^{-1}, concentration 1×10^{-3} M, in DMSO for reduction and in acetonitrile for oxidation.

Table VII. Electrochemical Data for the $[CuM(L1)](ClO_4)_2$ Complexes[a]

compd	redn $E_{1/2}$/V (ΔE/V)		oxidn[b] E_a/V	
1a	−0.90 (0.06)			+1.42
3a	−0.87 (0.08)			+1.24
4	−0.76 (0.07)		+0.64	+1.39
5a	−0.76 (0.07)			+1.25
6	−0.92 (0.06)	−0.76 (0.06)		+1.30
7	−1.09	−0.35 (0.12)		+1.37
8	−0.81 (0.07)			+1.36

[a] In DMSO for reduction and in acetonitrile for oxidation (concentration 1×10^{-3} M); supporting electrolyte TEAP (0.1 M); scan rate 50 mV/s; glassy-carbon working electrode; Pt auxiliary electrode; SCE reference electrode. [b] Anodic peak being given.

dimethyl sulfoxide (DMSO) for reduction and in acetonitrile for oxidation. Typical cyclic voltammograms are given in Figure 11, and the numerical data are summarized in Table VII.

The CuM complexes, except for the Cu_2 complex **7**, show a pseudoreversible couple near −0.9 V which may be ascribed to reduction of the Cu center.[13,14a,b,15,16] This wave was found to involve a one-electron transfer on the basis of coulometry studies for the CuMn complex **3a**. The electrolyzed solution of **3a** assumes a yellow color and shows no absorption in the visible region (see Figure 9, trace b). Further, the electrolyzed solution shows a rhombic ESR signal with six-lined hyperfine structure ($A_{iso} = 93$ G) near $g = 2.0$ that is typical of Mn(II) ion ($I_{Mn} = {}^5/_2$). Evidently, the reduction occurs at the Cu(II) center, i.e., $Cu^{II}Mn^{II}/Cu^{I}Mn^{II}$. In the cyclic voltammogram of the CuNi complex **6**, a second reduction appears at −0.92 V which is tentatively assigned to the reduction at the Ni(II) center.[14c]

In the cyclic voltammogram of the Cu_2 complex **7**, two reduction waves are observed at −0.35 and −1.09 V. It is reasonable to assign the wave at −0.35 V to the reduction of Cu(II) at the 5-coordination site and the wave at −1.09 V to the reduction of Cu(II) at the 4-coordination site. It should be noted that the reduction of Cu(II) occurs at a negative potential relative to that of the other CuM complexes. This is because the reduction of Cu(II) accompanies the charge change from 1+ to 0 in **7** ($[Cu^{II}Cu^{I}]^+ \rightarrow [Cu^{I}Cu^{I}]^0$) compared with the change from 2+ to 1+ in the other CuM complexes ($[Cu^{II}M^{II}]^{2+} \rightarrow [Cu^{I}M^{II}]^+$). In this connection, it should be pointed out that the reduction of (*N,N'*-ethylenedisalicylideneaminato)copper(II) [Cu(salen)], which is compared to Cu(II) at the 4-coordination site of the CuM complexes, occurs at a more lower potential[44] because this reduction accompanies the charge change from 0 to −1. Our attempts to synthesize a $Cu^{II}Cu^{I}$ complex of L1 were unsuccessful because controlled-potential electrolyses at −0.35 V resulted in the deposit of metallic copper on the electrode.

In the sweep in the positive potential, all the complexes showed an irreversible wave near +1.3 V. This wave involves a one-electron transfer on the basis of coulometry experiments for **3a**. However, this wave cannot be attributed to the oxidation at the Cu(II) center since related mononuclear Cu(II) and dinuclear $Cu^{II}M^{II}$ complexes show no oxidation associated with the Cu at such a low potential. The electronic spectrum of the electrolyzed solution of **3a** is given by trace c in Figure 10, in which the d–d band of Cu(II) remains intact at 547 nm. Notable spectral changes of the oxidation are the appearance of a weak band near 420 nm and the decrease in intensity of the π–π^* band. On the basis of these facts, we presume that the oxidation near +1.3 V occurs at one C=N linkage of the macrocycle L1.

In the cyclic voltammogram of the CuFe complex **4**, an irreversible wave appears at +0.64 V that is assigned to the oxidation of Fe(II): $Cu^{II}Fe^{II}/Cu^{II}Fe^{III}$.[14a,b] On the other hand, the CuMn (**3a**) and CuCo (**5a**) complexes show no oxidation wave attributable to the Mn(II) and Co(II) center below +1.3 V. It should be emphasized that the dinuclear Mn(II) complex of macrocycle I ($m = n = 3$) shows the Mn(II)/Mn(III) oxidation wave at +0.55 V (in DMF).[14a,b] Both **3a** and **5a** showed an irreversible wave near +1.5 V, but the assignment of the wave was not done in this study. The highly distorted configuration about the Mn(II) and the elongated Mn(II)–ligand bonds, as proved in our X-ray structure analysis for **3a**, are certainly associated with the stabilization of the Mn(II) oxidation state in the present CuMn complexes. This must be also the case for the stabilized Co(II) state in **5a**. Thus, the present study illustrates that the macrocyclic ligand provides a specific geometrical environment for bound metal ions and influences their electrochemical behaviors.

Acknowledgment. This work was partly supported by a Grant-in-Aid for Scientific Research on Priority Area (No. 03241105).

Supplementary Material Available: Positional and thermal parameters of non-hydrogen atoms (Tables S2 and S6), hydrogen atom locations (Tables S3 and S7), and bond distances and angles (Tables S4 and S8) for **1c** and **3c**, respectively, numerical data for the magnetic susceptibilities of **3a–c**, **4**, **5a,b**, **6**, and **7** (Tables S9 and S10), magnetic best-fittings for **3a,c** and **5b** (Figures S1–S3), and ESR for the Cu(I)–Mn(II) complex (Figure S4) (16 pages). Ordering information is given on any current masthead page.

(44) Patterson, G. S.; Holm, R. H. *Bioinorg. Chem.* **1975**, *4*, 257.